# ChemComm

Accepted Manuscript


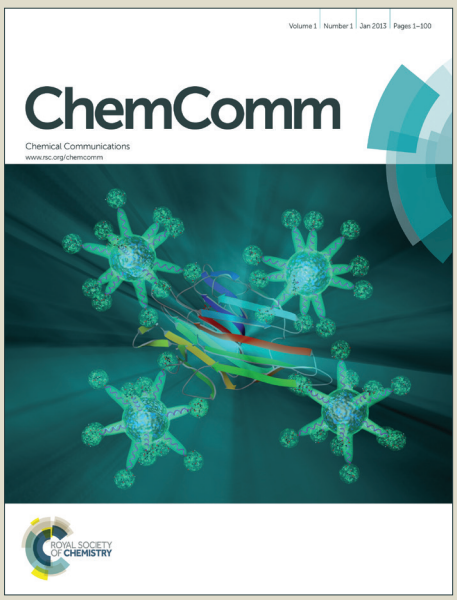





ROYAL SOCIETY OF CHEMISTRY

www.rsc.org/chemcomm

Journal Name ChemComm Dynamic Article Links ►

Cite this: DOI: 10.1039/c0xx00000x

www.rsc.org/xxxxxx

ARTICLE TYPE

# P22 Virus-like Particles Constructed Au/CdS Plasmonic Photocatalytic Nanostructures for Enhanced Photoactivity

**Ziyou Zhou[a], Gregory J. Bedwell[b], Rui Li[b], Ningzhong Bao[c], Peter E. Prevelige, Jr.[b]*, and Arunava Gupta[a]***

***Received (in XXX, XXX) Xth XXXXXXXXX 20XX, Accepted Xth XXXXXXXXX 20XX***
**DOI: 10.1039/b000000x**

**Plasmonic photocatalytic nanostructures have been fabricated under mild conditions (room temperature aqueous solution) using genetically engineered bacteriophage P22 virus-like particles (VLP) as a nano-platform. The photodegradation of methylene blue by CdS photocatalyst confined inside VLP can be significantly enhanced by the controlled deposition of gold nanoparticles on the outer shell of VLP-CdS.**

Photocatalysis using solar radiation represents a promising route for the development of renewable energy sources (e.g., $H_2$ production) and environmental remediation (e.g., $CO_2$ reduction).[1-2] For traditional photocatalysts, the potential obstacles are low light harvesting efficiency and unwanted charge recombination.[3] An attractive strategy to address these issues is to incorporate noble metals (e.g., Ag, Au) into the photocatalytic system, thus creating so-called plasmonic photocatalytic nanostructures.[4-7] The incorporated noble metals, e.g. gold nanoparticles, have shown to significantly improve the performance of photocatalysts by strongly absorbing visible light due to surface plasmon resonance (SPR), and preventing the photo-generated holes and electrons from recombination.[8-10]

Herein, we report on the use of virus-like particles (VLP), which are derived from assemblies of virus protein subunits lacking the viral genome, as nano-platforms for the controlled fabrication of plasmonic photocatalytic nanostructures. VLP have attracted attention in developing exquisite functional nanomaterials due to their wide availability, easy controllability and facile manipulability.[11-14] VLP with precise three dimensional nanostructures display a wide variety of shapes and structures, and can be produced in large quantities using standard biological amplification and growth protocols. Both the exterior and interior surfaces of the VLP can be functionalized by genetically or chemically modifying the protein subunits, which is desirable for the controlled construction of nano-architectures with multiple components.[15-18] We have been interested in using bacteriophage P22 as a nano-platform for functional materials design and synthesis, and in recent work have demonstrated its robustness and versatility as a biotemplate for the synthesis of a wide range of ordered nanomaterials.[19-21] P22 VLP can withstand relatively high temperatures (up to 80 °C), stable over a wider range of pH than most other VLP, and are non-infectious.[22] The most fascinating aspect of P22 is its unique nanoarchitecture, composed of a shell assembled from 420 copies of a coat protein (CP) and an interior cavity containing approximately 300 copies of a scaffolding protein (SP).[20] These features provide tremendous versatility for P22-based materials design and fabrication. Successful examples include ordered synthesis and directed assembly of sulphides on shells of P22 VLP by engineering coat protein and confined synthesis of a wide range of nanomaterials inside the interior cavity of P22 VLP by manipulating the scaffolding proteins.[19, 21, 23-26] Exploiting both the coat and scaffolding proteins further offers the opportunity of fabricating multifunctional structures for specific applications.

In this communication we demonstrate a P22 VLP-based strategy for constructing plasmonic photocatalytic nanostructures using a three-step procedure: 1) self-assembly of spherical VLP from P22 wild-type CP and genetically engineered truncated SP; 2) selective synthesis of photocatalytic nanocrystals at the engineered SP sites positioned in the inner cavity of assembled spherical P22 templates; and 3) nucleation and growth of plasmonic noble metal nanostructures on the CP. As a model system we have used CdS as the photocatalyst and gold as the plasmonic metal. The synthetic strategy we have developed is quite general and can be extended to fabricate a variety of other plasmonic photocatalytic nanomaterial systems.

Figure 1 demonstrates the assembly of genetically engineered P22 VLP, the confined growth of CdS nanocrystals inside the inner cavity, followed by nucleation and formation of gold nanoparticles on the surface of VLP. The assembly process and the resultant VLP structure are similar to those of wild-type P22 procapsid. Typically, 420 copies of the P22 coat protein (47 kDa) assemble with the aid of approximately 300 copies of truncated genetically engineered scaffolding protein (19 KDa) to form an icosahedral T=7 P22 VLP (Figure 1a). Based on 50 randomly selected particles, the protein assembly has been established to have an average diameter of 60 nm, which is in agreement with the size of wild type P22 procapsid.[22] A peptide sequence with strong affinity for CdS (SLTPLTTSHLRS), previously identified from a phage display peptide library by Belcher's group,[27-28] is genetically fused into the SP and are confined inside the resultant VLP. In a typical inorganic synthesis, the protein-directed nucleation of CdS nanocrystals occurs at the engineered regions of SP. Thus, an engineered protein assembly is capable of initially forming approximately 300 isolated CdS nanocrystals

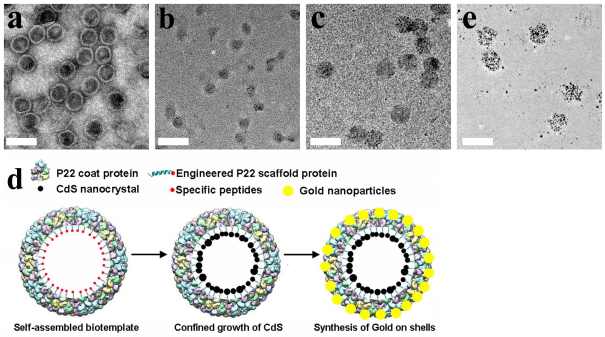


**Figure 1.** TEM images of a) genetically engineered P22 VLP, stained with 2% uranyl acetate; b) CdS confined inside P22 VLP, unstained; c) Au/CdS core/shell structure constructed using P22 VLP nanoplatform, unstained; and e) growth of Au on the surface P22 VLP without CdS, unstained. d) Schematic illustration of the formation of Au/CdS core/shell structure using genetically engineered P22 VLP. Step 1: assembly of P22 VLP genetically engineered with specific peptide (red); step 2: Site-directed nucleation and growth of CdS (black) on the engineered scaffolding protein that are confined inside VLP; step 3: selective formation of gold nanoparticles on the surface of VLP. All scale bars represent 100 nm.

distributed inside the P22 VLP. We have previously reported that the confined synthesis of CdS inside P22 VLP can be manipulated by the kinetically controlled release of sulphur from thioacetamide precursor introduced into a solution of the VLP and cadmium ions.[23] Using the previously reported protocol[23] we prepared a transmission electron microscopy (TEM) sample after CdS growth for 3 hours. The result (Figure 1b) shows that the unstained VLP-CdS nanostructures have a size around 40 nm, which is in accordance with the dimension of the inner cavity of P22. This suggests that the formation of CdS occurs exclusively inside the P22 VLP and the outer shell remains intact, or else the size of resultant P22-CdS would have been around 60 nm. The intact outer shell then serves as an ideal platform for added incorporation of plasmonic gold nanoparticles.

The resultant CdS-VLP assembly is consequently purified and re-suspended in DI water for further selective growth of gold nanoparticles on the outer surface of the VLP. Figure 1c presents TEM images (without staining) of the Au-VLP-CdS nanostructures (gold precursor concentration in the reactant solution is 35 μM), which have a dimension of around 60 nm that is very close to the size of P22 VLP before any materials synthesis. This suggests that the formation and growth of gold likely occurs at the lower ridges of the uneven P22 VLP surface,[29] explaining why there is no notable size increase. Since both CdS and Au have high atomic number, it is difficult to clearly differentiate them in Figure 1c. To demonstrate that gold nanoparticles can be selectively deposited on the surface of VLP, we synthesized gold using engineered VLP without the formation of CdS. Using the same concentration of gold precursor, we obtained discrete gold nanoparticles on the surface of VLP (as shown in Figure 1e) with notably different contrast as compared to that of the imaged Au-VLP-CdS nanostructures. By randomly selecting 50 Au-VLP nanoparticles, we determined their average size to be around 60 nm, which is very similar to that of P22 VLP as well as that of Au-VLP-CdS. The size distribution of P22 VLP, VLP-CdS, Au-VLP-CdS, and Au-VLP are presented in Figure S1, from which we ascertain that the stained P22 VLP have an average dimension significantly larger than that of unstained VLP-CdS, while being similar to that of both unstained Au-VLP-CdS and Au-VLP. This conclusively confirms that the synthesis of CdS is confined inside the P22 VLP and has limited influence on the subsequent deposition of gold nanoparticles on the outer shell of VLP.

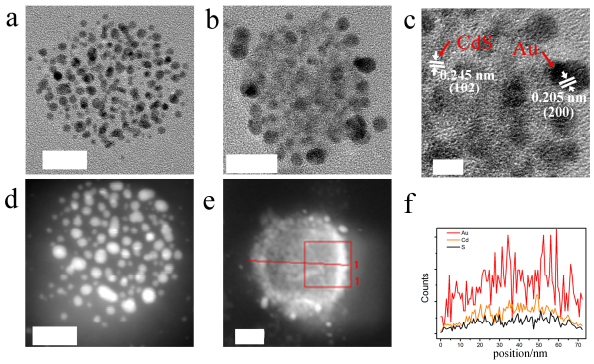


Figure 2. TEM images of (a) Au-VLP and (b) Au-VLP-CdS. (c) HRTEM image of Au-VLP-CdS. STEM images of (d) Au-VLP and (e) Au-VLP-CdS. (f) Drift corrected elemental spectral profile for Au-VLP-CdS. All scale bars represent 20 nm, except for figure 2c, in which scale bar represents 5 nm.

To further verify that gold nanoparticles are present on the surface of VLP-CdS, we have carried out HRTEM (high resolution TEM) and STEM (scanning transmission electron microscopy) measurements to examine and compare in detail the structure of Au-VLP and Au-VLP-CdS. In Figure 2a, the observed discontinuous contrast can be attributed exclusively to gold nanoparticles, since protein templates composed of non-conductive and light elements do not provide much contrast. In Figure 2b, the contrast is produced by both gold and CdS. This is the reason that we observe different degrees of contrast. At even higher magnifications used for obtaining detailed structural information of Au-VLP-CdS we observe two different sets of lattice fringes as indicated in Figure 2c. Lattice fringes with a spacing of $d$ = 0.245 nm correspond to the (102) planes of the wurtzite (hexagonal) structure of CdS (JCPDS card No. 80-0006), and lattice fringes with a spacing of $d$ = 0.205 nm correspond to the (200) planes of the face-centred cubic structure of gold (JCPDS, card No. 04-0784). STEM images also present distinctly different contrast for Au-VLP-CdS and VLP-CdS, as shown in Figure 2d and Figure 2e, respectively. We have further investigated the elemental composition of the as-obtained Au-VLP-CdS nanostructures by energy dispersive x-ray spectroscopy (EDX) measurements, in which signals from all three elements (Au, Cd, and S) can been detected, as shown in Figure 2f. The fluctuating characteristics of the spectral profiles for all the elements are consistent with the fact that both the gold and CdS nanoparticles are discrete rather than continuous over the protein templates, in agreement with our previous results using P22 VLP for crystal growth.[21, 23] The HRTEM, STEM and EDX results convincingly demonstrate that the gold and CdS are selectively deposited outside and inside the P22 VLP template, respectively.

We have further explored the controllability of gold formation on P22 VLP. Previously, Slocik and co-workers have shown that histidine-rich cowpea chlorotic mottle virus (CCMV) can direct the growth of gold in ordered periodic patterns, which they have termed as symmetry-directed synthesis.[30] The outer shell of the P22 VLP is composed of 420 copies of CP and each CP has two histidine residues, which likely can also direct the growth of gold. Based on the TEM image in Figure 3a, we indeed observe fairly uniform nucleation and growth of gold in a highly ordered manner when using a very low concentration of gold precursor (35 μM). Small gold nanocrystals with an average size of 2.8 nm, as estimated from 50 randomly selected assemblies, are uniformly distributed on the shells of P22 VLP. Based on the size and distribution of gold on P22 VLP we propose that the formation of gold templated by P22 VLP follows the symmetry-directed pathway - each CP binds with one or two gold nanoparticles (depending on the extent of exposure of histidine residues to gold) and CPs collectively direct the periodic ordering of gold. Since P22 shells are composed of 420 copies of CP, each consisting of two histidine residues, there are theoretically 420 to 840 sites on each VLP shell for gold nucleation and growth. Using imageJ software the number of gold nanocrystals on VLP surface is counted to be 230 (Figure 3a), which is within the range expected to be observed if 420 to 840 points are projected onto a plane (≥210). By increasing the gold precursor concentration, the size of gold nanoparticles can be well tuned from about 2.8 nm (35 μM), 4.4 nm (70 μM), 5.2 nm (105 μM), 8.4 nm (140 μM), and 8.7 nm (175 μM), as shown in Figure 3 and the size distribution provided in Figure S2. The growth of gold is also investigated by in-situ UV-Vis measurements and the results are shown in Figure S3. We have calculated the size of the gold nanoparticles from the intensity of absorption peaks and concentration of the gold precursor using a model proposed by Haiss et al.[31] Based on these calculations, the average size is determined to be 3.3 nm for a precursor concentration of 35 μM and 7.6 nm when the concentration is 175 μM, as shown in Figure S4. Overall, the results agree well with those determined by TEM.

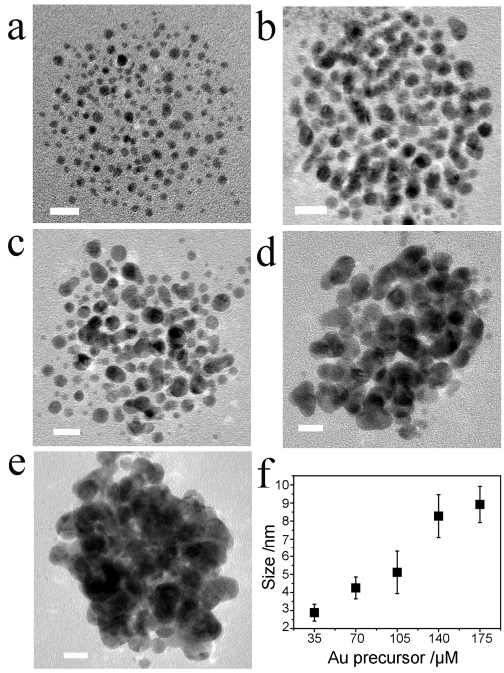


**Figure 3**. TEM images of the controlled synthesis of gold nanoparticles on the outer surface of engineered P22 VLP with different concentrations of gold precursor: a) 35 μM, b) 70 μM, c) 105 μM, d) 140 μM, and e) 170 μM. f) Calculated size of gold nanoparticles as a function of precursor concentration. TEM samples were prepared after reaction time of 5 minutes. All scale bars represent 10 nm.

We evaluated the photoactivity of the resultant CdS/Au nanocomposite by studying the photodegradation of methylene blue (MB) using a solar simulator system.[32] Figure 4 depicts the decay profiles of MB absorption at 660 nm, both with and without the photocatalyst. For all the different reactions the experimentally observed decrease in the MB concentration with time can be fitted well by an exponential, corresponding to first order reaction kinetics. For the photodegradation of MB with only protein, the rate constant $k_1$ is ~$2.6*10^{-3}$ $min^{-1}$, while in the presence of P22 VLP with gold on the outer shell, the rate constant $k_2$ is ~$4.9*10^{-3}$ $min^{-1}$. With CdS confined inside P22 VLP, the rate constant for MB degradation increases considerably to ~$1.6*10^{-2}$ $min^{-1}$. When gold nanoparticles are incorporated onto the VLP-CdS nanostructure, the photodegradation rate constants are further enhanced to $3.0*10^{-2}$ $min^{-1}$ and $3.5*10^{-2}$ $min^{-1}$ for gold nanoparticle size of 6.2 nm and 8.3 nm, respectively.

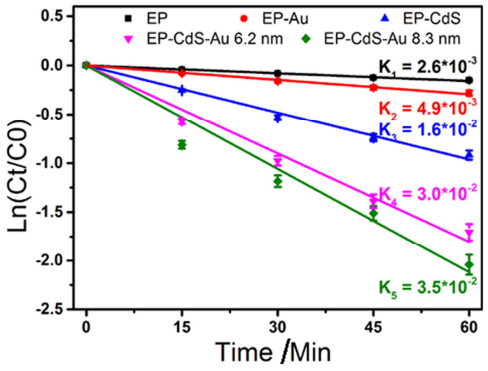


**Figure 4**. UV kinetic studies of the photodegradation of methylene blue (MB). EP: engineered P22 VLP. Ct: the concentration of MB at measured time; C0: the original concentration of MB (n=3 independent experiments, error bars represent ± S.D).

We have further carried out a series of experiments to evaluate the gold size-dependent photodegradation activity of MB, and the results are shown in Figure S5. We find that merely gold on the surface of P22 VLP does not affect the rate constant of photodegradation, while gold nanoparticles on VLP-CdS have a notable influence, with the rate constant increasing dramatically as the size of gold particle increases. Based on these results, we propose that it is the interaction between the gold and CdS that affects the photodegradation of MB. Radiative energy transfer can take place from gold nanoparticles to CdS through the strong surface plasmonic resonance (SPR)-induced electric field localized in the vicinity of the noble metal. Thereby the exciton population in the photocatalyst is substantially increased. The interaction is further enhanced with increasing size of gold

nanoparticles, which is in agreement with the well-known fact that localized surface plasmonic resonance (LSPR) of gold nanoparticles is size dependent.[33] The increased LSPR effect contributes to stronger absorption of visible light and the excitation of active charge carriers for enhanced photodegradation of MB.[5, 10, 34] Another possibility for photoactivity enhancement with increasing size of Au is the likelihood for gold nanoparticles to penetrate the soft protein layer and contact directly with CdS, thereby preventing electron-hole recombination and promoting the photoactivity of semiconducting photocatalyst.[10]

In conclusion, we have demonstrated that genetically engineered P22 VLP acts as a robust nano-platform for fabricating gold/CdS plasmonic photocatalytic nanostructures. The controlled formation of gold nanoparticles on the outer shell of VLP-CdS dramatically enhances the photoactivity of CdS confined inside the VLP. However, the gold nanoparticles by themselves exhibit no notable effect on the photodegradation of MB. These findings are relevant for the synthesis of a wide range of alternative plasmonic photocatalytic materials with desired components, architectures, and performance. This research was supported by the U.S. Department of Energy, Office of Basic Energy Sciences, Division of Materials Sciences and Engineering under Award No. DE-FG02-08ER46537.

## Notes and references

[a] *Department of Chemical and Biological Engineering, The University of Alabama, Tuscaloosa, AL 35487, United States. E-mail: agupta@mint.ua.edu; Fax: +1-2053482346;Tel: +12053483822*
[b] *Department of Microbiology, University of Alabama, Birmingham, Birmingham, AL 35294-2170, USA. E-mail: prevelig@uab.edu; Fax: +1 2059755479; Tel: +1 2059755327*
[c] *State Key Laboratory of Materials-Oriented Chemical Engineering, College of Chemistry and Chemical Engineering, Nanjing University of Technology, Nanjing 210009, China*

† Electronic Supplementary Information (ESI) available: See DOI: 10.1039/b000000x/

1. A. Kudo and Y. Miseki, *Chem. Soc. Rev.*, 2009, **38**, 253-278.
2. X. Wang, K. Maeda, A. Thomas, K. Takanabe, G. Xin, J. M. Carlsson, K. Domen and M. Antonietti, *Nat. Mater.*, 2009, **8**, 76-80.
3. X. Chen, S. Shen, L. Guo and S. S. Mao, *Chem. Rev.*, 2010, **110**, 6503-6570.
4. H. Zhang, X. Fan, X. Quan, S. Chen and H. Yu, *Environ. Sci. Technol.*, 2011, **45**, 5731-5736.
5. K. Awazu, M. Fujimaki, C. Rockstuhl, J. Tominaga, H. Murakami, Y. Ohki, N. Yoshida and T. Watanabe, *J. Am. Chem. Soc.*, 2008, **130**, 1676-1680.
6. J. Yu, G. Dai and B. Huang, *J. Phys. Chem. C*, 2009, **113**, 16394-16401.
7. P. Wang, B. Huang, X. Qin, X. Zhang, Y. Dai, J. Wei and M. H. Whangbo, *Angew. Chem.Int. Edit.*, 2008, **47**, 7931-7933.
8. E. Kowalska, O. O. P. Mahaney, R. Abe and B. Ohtani, *Phys. Chem. Chem. Phys.*, 2010, **12**, 2344-2355.
9. Y. Tian and T. Tatsuma, *J. Am. Chem. Soc.*, 2005, **127**, 7632-7637.
10. Z. W. Seh, S. Liu, M. Low, S. Y. Zhang, Z. Liu, A. Mlayah and M. Y. Han, *Adv. Mater.*, 2012, **24**, 2310-2314.
11. M. Brasch, A. de la Escosura, Y. Ma, C. Uetrecht, A. J. Heck, T. Torres and J. J. Cornelissen, *J. Am. Chem. Soc.*, 2011, **133**, 6878-6881.
12. F. Li and Q. Wang, *Small*, 2014, **10**, 230-245.
13. L. A. Lee, Z. Niu and Q. Wang, *Nano Res.*, 2009, **2**, 349-364.
14. N. F. Steinmetz, *Mol. Pharm.*, 2013, **10**, 1-2.
15. Q. Wang, T. Lin, L. Tang, J. E. Johnson and M. Finn, *Angew. Chem. Int. Edit.*, 2002, **41**, 459-462.
16. A. Kale, Y. Bao, Z. Zhou, P. E. Prevelige and A. Gupta, *Nanotechnology*, 2013, **24**, 045603.
17. J. E. Glasgow, S. L. Capehart, M. B. Francis and D. Tullman-Ercek, *ACS Nano*, 2012, **6**, 8658-8664.
18. N. Stephanopoulos, M. Liu, G. J. Tong, Z. Li, Y. Liu, H. Yan and M. B. Francis, *Nano Lett.*, 2010, **10**, 2714-2720.
19. S. Qazi, L. O. Liepold, M. J. Abedin, B. Johnson, P. Prevelige, J. A. Frank and T. Douglas, *Mol. Pharm.*, 2012, **10**, 11-17.
20. S. Kang, M. Uchida, A. O'Neil, R. Li, P. E. Prevelige and T. Douglas, *Biomacromolecules*, 2010, **11**, 2804-2809.
21. L. Shen, N. Bao, P. E. Prevelige and A. Gupta, *J. Am. Chem. Soc.*, 2010, **132**, 17354-17357.
22. D. P. Patterson, P. E. Prevelige and T. Douglas, *ACS Nano*, 2012, **6**, 5000-5009.
23. Z. Zhou, G. J. Bedwell, R. Li, P. E. Prevelige and A. Gupta, *Sci. Rep.*, 2014, **4**,3832 .
24. A. O'Neil, P. E. Prevelige, G. Basu and T. Douglas, *Biomacromolecules*, 2012, **13**, 3902-3907.
25. D. P. Patterson, B. LaFrance and T. Douglas, *Chem. Commun.*, 2013, **49**, 10412-10414.
26. M. Uchida, D. S. Morris, S. Kang, C. C. Jolley, J. Lucon, L. O. Liepold, B. LaFrance, P. E. Prevelige Jr. and T. Douglas, *Langmuir*, 2011, **28**, 1998-2006.
27. C. Mao, D. J. Solis, B. D. Reiss, S. T. Kottmann, R. Y. Sweeney, A. Hayhurst, G. Georgiou, B. Iverson and A. M. Belcher, *Science*, 2004, **303**, 213-217.
28. C. E. Flynn, C. Mao, A. Hayhurst, J. L. Williams, G. Georgiou, B. Iverson and A. M. Belcher, *J. Mater. Chem.*, 2003, **13**, 2414-2421.
29. K. N. Parent, R. Khayat, L. H. Tu, M. M. Suhanovsky, J. R. Cortines, C. M. Teschke, J. E. Johnson and T. S. Baker, *Structure*, 2010, **18**, 390-401.
30. J. M. Slocik, R. R. Naik, M. O. Stone and D. W. Wright, *J. Mater. Chem.*, 2005, **15**, 749-753.
31. W. Haiss, N. T. Thanh, J. Aveyard and D. G. Fernig, *Anal. Chem.*, 2007, **79**, 4215-4221.
32. L. M. Shen, N. Z. Bao, P. E. Prevelige and A. Gupta, *J. Phys. Chem. C*, 2010, **114**, 2551-2559.
33. J. M. Zook, V. Rastogi, R. I. MacCuspie, A. M. Keene and J. Fagan, *ACS Nano*, 2011, **5**, 8070-8079.
34. C. Hu, T. W. Peng, X. X. Hu, Y. L. Nie, X. F. Zhou, J. H. Qu and H. He, *J. Am. Chem. Soc.*, 2010, **132**, 857-862.